Kinetics of ordering in two dimensions. II. Quenched systems

Paramdeep S. Sahni, David J. Srolovitz, Gary S. Grest, Michael P. Anderson, and S. A. Safran
Corporate Research Science Laboratories, Exxon Research and Engineering, Linden, New Jersey 07036
(Received 22 March 1983)

An efficient Monte Carlo procedure is applied to the study of the kinetics of low- and high-Q Potts models on surfaces quenched from a high temperature ($T \gg T_c$) to low temperatures ($T < T_c$). The kinetics of these models are analyzed in simulations which yield the time dependence of the size and shape of the domains. After an initial transient period, the mean domain size R increases with time as $R \sim t^n$. For the triangular lattice at all temperatures and for the square lattice at temperatures $T > 0.5T_c$, the exponent n decreases from $\frac{1}{2}$ for $Q=2$ (Ising model) to approximately 0.41 for large Q. The distribution of grain sizes and shapes is also calculated from the results of the simulations. For large Q, these distributions are time independent. On the square lattice at low temperatures the growth exponent is approximately equal to 0, due to the nucleation of pinned domains. The Monte Carlo results are discussed in terms of experimental studies of the ordering of adsorbed atoms on surfaces and of the growth of grains in polycrystalline materials.

I. INTRODUCTION

The kinetics of domain growth has a direct influence on polycrystalline microstructures and is a subject of considerable interest in surface science[1,2] and in metallurgy.[3] The development of long-range order in a system with more than one equilibrium state is fairly well understood for three-dimensional systems such as binary alloys[4–6] with two equivalent sublattices which are quenched from high to low temperatures. At high temperatures, there are no ordered regions even in equilibrium. A short time after a quench to low temperatures, the entire sample consists of domains of ordered regions. These domains grow due to curvature, and equilibrium is characterized by domains of macroscopic size. When the order parameter is conserved in three dimensions, the average domain size increases as the square root of the time (t), and this has been confirmed by both Monte Carlo (MC) simulations[5] and experiments[4] on alloys such as Fe-Al and Cu-Au. In two dimensions (i.e., on surfaces) the growth exponent remains unchanged,[6] but roughening fluctuations result in a strong temperature dependence to the growth rate, as shown in earlier papers.[7,8]

While systems with $Q=2$ degenerate ground states approach equilibrium in the manner described above, the situation for highly degenerate ($Q>2$) systems is not as simple. Examples of systems with $Q>2$ are found in the superlattice structures observed for adsorbed atoms on surfaces as discussed in the preceding paper, which we refer to as I. In addition, grain growth in crystals can be viewed as the $Q \to \infty$ limit of such models, in the approximation that all grain boundaries are energetically equivalent.[9] When $Q>2$, the effects of intersections of three or more domains must be considered in addition to the effects of curvature when analyzing the kinetics.[10] In the preceding paper it was shown that in two dimensions, for $Q>2$, it is possible for certain isolated domain geometries to remain frozen, with neither growth nor shrinking resulting in a decrease of the free energy. These results on isolated domains suggest that for systems with $Q>2$, the effects of domain-wall intersections can result in slower kinetics than the Ising-type ($Q=2$) systems. Of course, the extreme result of no growth is only to be expected when the completely pinned configurations discussed in the preceding paper are dominant in an actual quench.[11–13]

In this paper, we present a detailed Monte Carlo study of the kinetics of domain growth in two-dimensional systems quenched from high to low temperatures, for both small ($Q=3,4,6$) and large ($Q=12$–64) degeneracies. The two-dimensional case is studied since it requires a smaller number of lattice sites and because the topology of the domain configurations is easily visualized and analyzed. The results are directly applicable to the growth of superlattice structures in the adsorption of atoms on surfaces, where the Q-component Potts systems studied here have been shown to provide good models for the equilibrium phase transitions.[14] In addition, the high-Q results should be applicable to the growth of polycrystalline domains in thin films if surface grooving effects are unimportant. Finally, since the exponents obtained for growth of the average domain size as a function of time, are not related to fluctuation effects (i.e., they are obtained on the triangular lattice at $T=0$), it is possible that they are appropriate to the problems of three-dimensional ordering and grain growth as well.

The main results of this paper are (i) the analysis of the growth exponent n, defined by $R \sim t^n$, where R is the average linear domain size, and (ii) the demonstration of the time invariance of the distributions of domain sizes and shapes. For quenches on a triangular lattice at all temperatures and on a square lattice at high ($T > 0.5T_c$) temperatures, the growth exponent is shown to vary from $n=0.5$ for $Q=2$ to an apparently asymptotic value of $n \cong 0.41$ for high Q. This indicates the role of domain-wall intersections in slowing down the kinetics of the

high-Q systems. It is only on the square or honeycomb lattices with nearest-neighbor interactions and at low temperatures that the domain configuration remains completely frozen and the growth exponent is zero. When the system contains longer-range interactions, it is possible that the completely pinned configuration described in I is no longer stable, and that the exponent n is the same as for the triangular lattice. Preliminary versions of these results were presented in Refs. 15 and 16.

The organization of the paper is as follows. In Sec. II, we discuss the Monte Carlo model and procedure used for the high-Q simulations. An efficient algorithm for the spin-flip kinetics was necessary, since for high Q there are many possible spin flips that must be attempted. Section III contains our results for the lattice and Q dependence of the growth exponent. The temperature dependence of n is discussed as well and some simple arguments are presented to qualitatively explain the observed trends with lattice and with Q. The distribution of domain sizes and shapes is presented in Sec. IV, where the time invariance of the configurations is demonstrated. In addition, the Monte Carlo results are discussed in terms of experimental studies of domain sizes and distributions in metallurgical systems.[17] In particular, the normalized distribution function for the domain size is shown to much more accurately reproduce the experimentally observed[18] distribution than the theoretical distribution calculated by Hillert.[19]

II. MODEL AND MONTE CARLO METHOD

We studied the Q-component ferromagnetic Potts model with a nonconserved order parameter (Glauber dynamics),

$$H=-J\sum_{\mathrm{NN}}\delta_{S_i S_j}\ , \tag{1}$$

where S_i is the Q state of the spin on site i ($1\le S_i\le Q$) and $\delta_{i,j}$ is the Kronecker δ function. The sum is taken over all nearest-neighbor (NN) spins and $J>0$. In all of our simulations, we started the system in a high temperature state and rapidly quenched to $T<T_c$. To reduce boundary effects, we employed very large systems (200×200 sites for the triangular lattice and either 200×200 or 150×150 for the square lattice), and used periodic boundary conditions. Both standard MC methods[20] and a generalization of the Bortz, Kalos, and Lebowitz[21] "n-fold" technique for the Potts model were used, as described below.

Some of the $T=0$ data and all of the $T>0$ data were obtained using standard MC methods, with Glauber dynamics.[20] In this method, both the spin and a new trial spin orientation were chosen at random. The transition probability W is given by

$$W=\begin{cases}\exp(-\Delta E/kT), & \Delta E>0\\ 1, & \Delta E\le 0\end{cases} \tag{2}$$

where ΔE is the change in energy caused by the spin flip. We define the unit of time as 1 Monte Carlo step per spin (MCS/S) which corresponds to N microtrials or spin-flip attempts, where N is the total number of spins. The data quoted below represent averages, taken over at least five runs. We found that it was very useful to store an array of size $L\times L\times Q$ which contained for each site the number of nearest neighbors of each Potts spin of orientation Q. At $T=0$ a spin flip is successful only if ΔE is less than or equal to zero. Thus considerable time was saved by not checking those spins for which more than half of the neighboring spins were of the same orientation. At late times, most of the spins were not on the boundary, and this lookup table saved considerable computer time, even though the table had to be updated whenever a spin was flipped.

At very low temperatures and high Q, the probability of flipping an arbitrary spin to a randomly chosen orientation is extremely small, since only a small number of the $(Q-1)$ other orientations of the spin have $\Delta E\le 0$. In order to overcome this problem, we have generalized the continuous-time method (n-fold way) developed by Bortz, Kalos, and Lebowitz[21] for the Ising model to the general Q Potts model. This method has recently been employed by Graim and Landau[22] for the study of three- to one-dimensional crossover in the Ising model. In the Ising ($Q=2$) version of this method, a spin is flipped at each trial and the time elapsed since the previous flip is calculated. Since every spin flip is successful, this method is more effective than the standard method at low temperatures. However, for $T>0$, it is only practical for very small Q, since one must keep track of all possible spin environments. This obviously grows rapidly with Q. Therefore, we have generalized this technique for the Potts model and employed it only for $T=0$.

We first review the method of Bortz *et al.*[21] for the Ising model ($Q=2$). The spins are first grouped into classes by their local environment. The probability of flipping any spin in a class is identical and equal to

$$p_i=\begin{cases}N_i\exp(-\Delta E/kT), & \Delta E>0\\ N_i, & \Delta E\le 0\end{cases} \tag{3}$$

where N_i is the number of spins in class i and the total probability is

$$P=\sum_i p_i\ . \tag{4}$$

Here N_c is the number of classes of spins and depends on the type of interactions included. A random number between zero and P is used to determine which class of spin shall be flipped and then a second random number is used to determine which of the spins in the class shall be flipped. The time since the previous flip is then

$$\Delta t=-\frac{\tau}{N}\ln R\ , \tag{5}$$

where R is a random number, $0<R<1$, and τ is the average time between attempted spin flips (one microtrial in the standard method). For their problem, Graim and Landau[22] have reported a factor of 10^4 net improvement at $T=T_c/2$ over the standard method.

This method can be readily generalized to the Potts model, but because of the large number of possible local environments for large Q, it is not obvious that it is practical. However, we have found that it is a very useful method for speeding up the calculation at $T=0$, where the

number of local environments which must be considered is greatly reduced. At $T=0$, there are basically only two classes of spins. The first class consists of those spins for which a flip to any of the $(Q-1)$ other orientations raises the energy and is therefore not allowed, $p_i=0$. The other class of spins are those for which at least one of the $(Q-1)$ orientations has $\Delta E \leq 0$. For the triangular lattice, most of the spins in this latter class can flip to either 1, 2, or 3 other spin orientations. The quantity P is then simply the sum over all sites of the number of orientations N_{fi}, each spin i can flip to

$$P=\sum_i N_{fi} \ . \tag{6}$$

A random number between 0 and P is used to determine which of the spins is flipped and a second random number is generated to determine which of the N_{fi} possible orientations will be chosen. The time since the previous flip is then computed as

$$\Delta t = -\frac{\tau(Q-1)}{P}\ln R \ . \tag{7}$$

The $(Q-1)$ factor enters, since in the standard MC method only $N_{fi}/(Q-1)$ attempted spin flips are ever successful. This formula reduces to the Ising result since for $Q=2$, $N_{fi}=0$ or 1. It also has the correct behavior at very high temperatures, where $N_{fi}=(Q-1)$ for every spin, in which case $P=N(Q-1)$. Then as expected $\langle \Delta t \rangle = \tau/N$ since $\langle \ln R \rangle = -1$. For $T>0$, the probability for flipping a spin to each and every one of the other $(Q-1)$ orientations would also have to be included in the computation of P. While this is easy to include for small Q, most of the gain in computer time would be lost in the necessity of keeping track of a large number of local environments. We found this technique to be valuable in the late stages of the domain growth when most of the sites are bulk sites and therefore cannot be flipped. In the very early stages of the growth, immediately after the quench, this method was in fact slower than the standard procedure, since almost every spin is flipped. Thus in the first few MC steps after the quench, we used the standard MC method, switching over to the continous-time method when $P \lesssim N/5$. This new procedure was particularly useful in following the domain growth out to long times, since the computer time per MCS/S decreased as the number of boundary sites decreased. This was not true of the standard MC procedure since it had to check all sites with equal probability even though most of them would not flip. Finally, we also were able to speed up the continuous-time method even further by generating a table of those spins which were not surrounded entirely by like neighbors. This table was updated after each MCS/S and this limited the number of spins which had to be checked during the run. As a check on the method and our program, we carried out an extensive test of the new method. Results for $Q=12$ and 36 were obtained by both methods and averaged over five configurations. The results for the average domain area versus time were in excellent agreement.

III. KINETICS OF DOMAIN GROWTH

In this section, we present the kinetic results of our Monte Carlo simulations of domain growth for both small and large Q, triangular and square lattices, for $T=0$ and finite temperatures. It is observed that for all Q on the triangular lattice, the domains are not pinned and that the growth exponent is independent of temperature. However, for $Q \geq 3$, the domains are pinned on the square lattice at $T=0$. These domains become progressively unpinned with increasing temperature; the growth ultimately approaching the kinetics observed on the triangular lattice. On the triangular lattice, at all temperatures, and on the square lattice, at elevated temperatures, the growth exponent is found to initially decrease with increasing Q and then become independent of Q for large Q.

A. $T=0$ kinetics

In Fig. 1 we display instantaneous spin configurations for the $Q=3$, 6, 12, and 64 Potts models on the triangular lattices that were quenched from high temperatures ($T \gg T_c$) to $T \cong 0$. Gross morphological changes occur as Q increases from near the Ising value ($Q=2$) toward the limit of an infinitely degenerate order parameter ($Q=\infty$). The low-Q configurations consist of very irregular and asymmetric domains; the irregularity increasing with decreasing Q. On the other hand, the domains in the high-Q configurations are significantly more compact and equiaxed. The cause of these large differences can be clarified by considering the possible modes of growth in the two limits. Figures 2 and 3 show the development of the observed morphologies for $Q=4$ and 64, respectively. Comparison of these two figures indicates that in the low-Q limit, large discontinuous changes in the area of individual grains can occur when one domain meets and coalesces with another domain with the same spin orientation. The probability of such chance meetings scales for

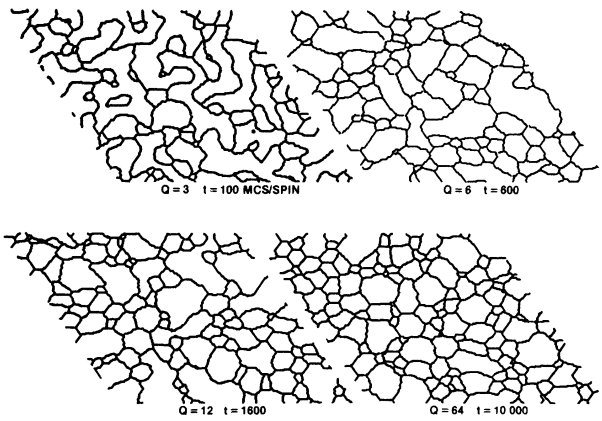

FIG. 1. Spin configurations for the $Q=3$, 6, 12, and 64 Potts model on a triangular lattice that were quenched from $T \gg T_c$ to $T \cong 0$. Solid curves represent the boundaries between regions of unlike spin. The times were chosen to yield comparable domain sizes.

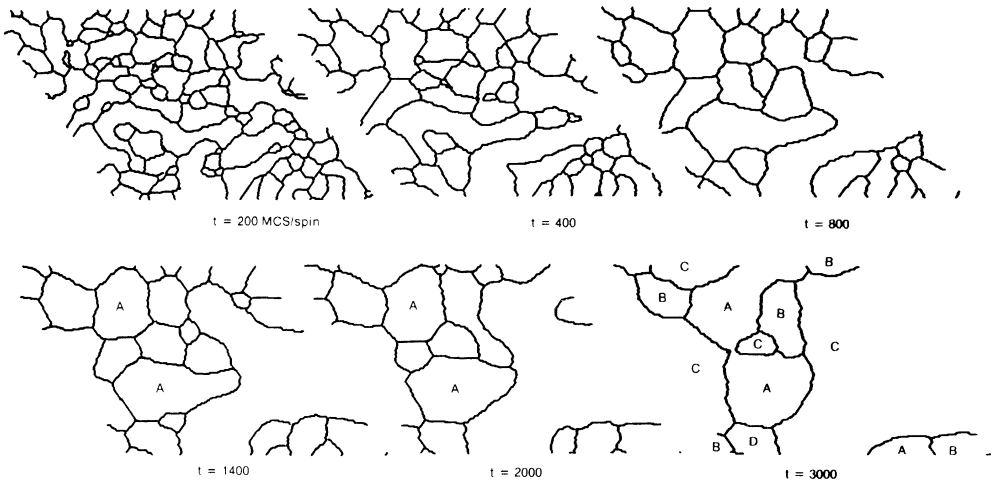

FIG. 2. Spin configurations for the $Q=4$ Potts model on a triangular lattice that was quenched to $T\cong 0$. In the bottom three configurations, the letters indicate spin orientation of the enclosing domain. The $t=3000$ configuration illustrates a coalescence event, where two domains of orientation A merge into a single domain.

large Q as Z/Q, where Z is the number of second-nearest-neighbor domains.[16] Since such coalescence events are strictly forbidden in the $Q=\infty$ case, the rarity of such events in the $Q=64$ simulations indicate that the infinitely degenerate system can be successfully modeled with a large finite value of Q. An example of a highly degenerate system can be found in the grain structure of polycrystalline materials, where the spin direction can be associated with the local orientation of the crystalline lattice.[23] This correspondence can be observed by comparing the configurations in Figs. 1(d) and 3 with the experimentally observed microstructure of the polycrystalline iron sample, reproduced in Fig. 4.

In analyzing the results of the present simulations, we monitored the mean area per grain $\langle A(t)\rangle$, which is simply related to the characteristic linear domain size $R(t)$. While $R(t)$ is most frequently calculated via structure factor analyses and $A(t)$ via cluster enumeration techniques, as in Sec. IV, we have adopted a new, much faster topological form of analysis. Using a generalized form of Euler's formula, we calculate the total number of domains $D(t)$ in terms of the number of edges $E(t)$ and vertices $V(t)$:

$$D(t)-E(t)+V(t)=\begin{cases}0 & \text{for infinite systems}\\ 1 & \text{for finite systems.}\end{cases} \tag{8}$$

Further, for an infinite system or one in which periodic boundary conditions are maintained, we know that every edge is two ended and each vertex three rayed, implying $2E(t)=3V(t)$ and therefore, $D(t)=V(t)/2$. Equivalently, the mean area is related to the total area A_T by

$$\langle A(t)\rangle=2A_T/V(t)\ . \tag{9}$$

Since the number of three-point vertices are much faster and simpler to compute than doing the cluster enumeration, we are able to obtain much better statistics for our kinetic analysis.

The time dependence of the mean domain size is commonly fitted to the expression

$$R^m-R_0^m=Bt\ , \tag{10}$$

where R_0 is the mean domain size at $t=0$. When $R\gg R_0$ Eq. (10) can be approximated as

$$R=Ct^n\ , \tag{11}$$

where $n=1/m$. Equation (11) is the form that is most commonly used in fitting experimental data, since n can be directly extracted from a plot of $\log_{10}(R)$ vs $\log_{10}(t)$ at long times (Fig. 5). The power-law behavior was checked, in a few cases, by verifying the linearity of Eq. (10) for time ranges exceeding 10^4 MCS/S, where only a few

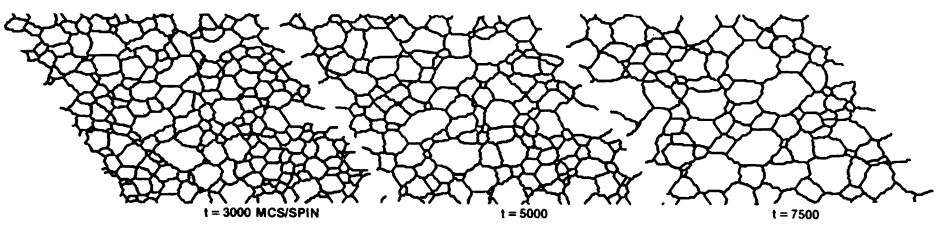

FIG. 3. Spin configurations for the $Q=64$ Potts model on a triangular lattice that was quenched to $T\cong 0$. Unlike in Fig. 2, coalescence events occur only rarely for this Q value.

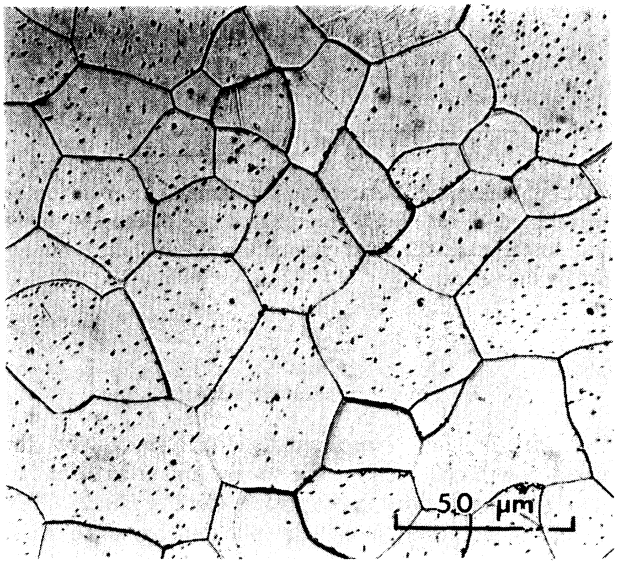

FIG. 4. Cross section of a high-purity polycrystalline iron sample which was etched to highlight the grain boundaries.

domains remained. The time dependence of the mean domain size was determined by monitoring the number of three-domain vertices during the simulation and employing Eq. (9). A nonlinear numerical fitting procedure was employed to calculate the exponent m in Eq. (10). In Fig. 6, we plot $n=1/m$ as a function of Q for the triangular lattice at $T\cong 0$. The exponent n is found to decrease linearly with increasing Q, for $Q<30$. Extrapolating this curve to the Ising limit ($Q=2$), we find that the well-known result ($n=\frac{1}{2}$) is reproduced. For $Q>30$, the exponent n is independent of Q and has a value of 0.41 ± 0.02. This value represents a slight increase over the exponent which we recently reported.[16] The difference is due to a slight programming error which has since been rectified. The Q independence of the exponent again suggests that it is possible to simulate infinitely degenerate systems with a Potts model with a finite Q. Because of the slight uncertainty in n implicit in the simulation, the sharpness of the transition of $n(Q)$ around $Q=30$ is unknown. For large Q, where the exponent n is constant, the prefactor C in Eq. (11) is found to be inversely proportional to $\sqrt{Q}$.

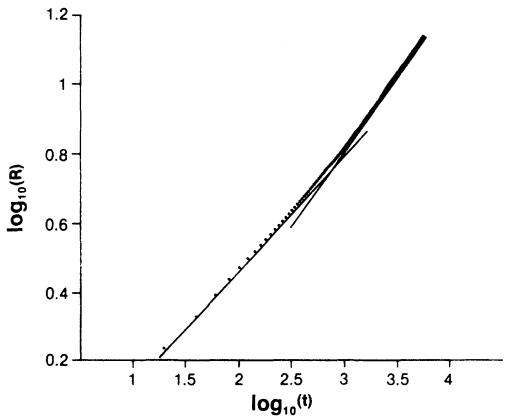

FIG. 5. Plot of $\log_{10}(R)$ vs $\log_{10}(t)$ for a $Q=48$ Potts model that was quenched to $T\cong 0$. Dots represent data that has been averaged over five simulations. Solid lines are fitted to either the short-time ($R\ll R_0$) or long-time ($R\gg R_0$) behavior. The exponent n is extracted from the slope of the long-time-fitted line.

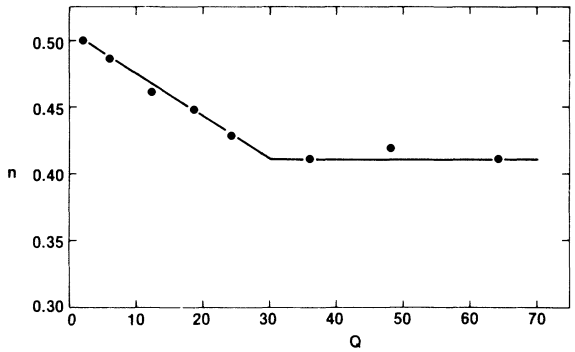

FIG. 6. Q dependence of the domain growth exponent n for the quenched Potts model on a triangular lattice.

In contrast to the triangular lattice, configurations on the square lattice reveal the symmetry of the underlying lattice. In Fig. 7 we display spin configurations for a $Q=6$ Potts model quenched from a high temperature to $T\cong 0$ on the square lattice. The spin configurations for the high-Q simulations on square lattices are not displayed since their growth is so slow that the number of boundary sites is of the same order as the number of bulk sites. As can be seen in the longer time configurations of Fig. 7, the domain sizes and morphology appear to be evolving toward a "frozen-in" configuration where all boundaries meet at 90° or 180° and have no curvature. Analyzing the kinetics as described above shows that the growth exponent n is zero for $Q\geq 3$. A growth exponent of zero is possibly indicative of logarithmic growth, as was predicted in the preceding paper on the basis of the evolution of simple domain configurations. Similar kinetics were also found for domain growth on a honeycomb lattice at $T\cong 0$. These observations are in accord with the predictions of Lifshitz[10] and Safran,[24] who suggested that the domains would be pinned for $Q\geq d+1$, where d is the dimensionality of the lattice. It should, however, be noted that $Q=d+1$ is the minimum Q value for which a pinning configuration can be developed. However, the mere existence of pinning configurations does not imply that the system is frozen, since it is neccesary that the pinning con-

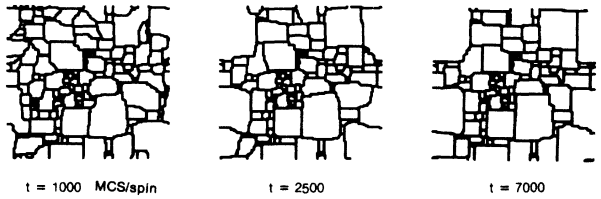

FIG. 7. Spin configuration for the $Q=6$ Potts model on a square lattice that was quenched from $T\gg T_c$ to $T\cong 0$.

figurations be nucleated in sufficient number to pin the entire structure.

In continuum models of domain growth, the driving force for growth is the reduction in curvature of the boundary. In lattice models, the curvature is discretized as kinks on the boundary. Such kinks can be annihilated by two distinct mechanisms: (1) two kinks of identical orientation (as defined by the lattice) and of opposite sign can meet and mutually annihilate, or (2) the absorption of a kink at a vertex where more than two grains meet. The first mechanism corresponds to purely curvature-driven growth, i.e., it can occur in Ising systems where no vertices are present. The second mechanism can only operate when vertices are present. Vertices, of zero-dimensional grain intersections, only exist provided that $Q \geq d+1$. In other words, by absorbing kinks, vertices are capable of reducing the curvature. This decrease in curvature slows down the domain growth, so that in the limit that all of the kinks have been absorbed, no domain growth is possible.

The ability of vertices to absorb kinks is a function of the detailed vertex configuration and kink orientation. On a square lattice all vertices are constructed such that the included angles are 90°, 90°, and 180° [Fig. 8(c)]. As is illustrated in Fig. 8, a kink on the vertical boundary is readily absorbed at the vertex. On the other hand, a kink on the horizontal boundary is neither absorbed or transmitted through the vertex (Fig. 9). Since a boundary can only end in a manner analogous to the vertical boundaries on Figs. 8 and 9, all boundaries are terminated on either end by kink-absorbing vertices. On a triangular lattice, three distinct types of vertex configurations exist; a 60°,60°,240° vertex, a 60°,120°,180° vertex, and a 120°,120°,120° vertex. The second two are illustrated in Fig. 10. However, it is easily shown[25] by line tension arguments that only the 120°,120°,120° vertex is stable. In Fig. 11, we illustrate the kink-vertex interaction for the triangular lattice. In this case, a kink in any of the three allowed orientations can move on two of the three boundaries that meet at a vertex. The vertex transmits a kink from one boundary to the next, regardless of its sign or orientation. Therefore, the difference in the kinetic behavior of domain growth on triangular and square lattices is determined by the kink-absorbing, and hence curvature-reducing, properties of the dominant vertex type.

FIG. 8. Schematic illustration of a vertex-kink reaction on the square lattice. A kink moving down the vertical boundary is absorbed at the vertex. The net result of the kink moving down the boundary and being absorbed is the horizontal translation of the vertical boundary by one lattice unit.

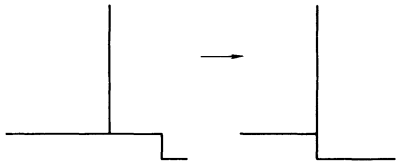

FIG. 9. Schematic illustration of a vertex-kink reaction on the square lattice for a kink traveling on one of the 180° boundaries. In this case, the kink, moving toward the left, is not absorbed by the vertex.

B. Finite-temperature kinetics

The kinetic and morphological differences in the domain growth observed on the square and triangular lattices at $T=0$ disappear as the temperature is raised. This, however, is not due to critical phenomena since these changes begin to occur at temperatures much lower than T_c. Figures 12 and 13 show spin configuration for $Q=4$ Potts models quenched from an initially high temperature ($T \gg T_c$) to $0.6T_c$ on triangular and square lattices, respectively. Unlike the $T=0$ studies, there are no discernable differences between the two lattices. The domain growth exponent n for the triangular lattice was found to be independent of temperature from $T=0$ to $T=0.7T_c$. Simulations at temperatures exceeding $0.7T_c$ were made; however, because of the large thermal fluctuations present, too many runs were required to obtain reliable data. We observed a decreasing prefactor [C in Eq. (11)] with increasing temperature. This result is in qualitative agreement with that found for the temperature dependence of the prefactor for the shrinking of a circular domain, analyzed in the preceding paper, and for the growth observed in Ising models.[6,8] In Figs. 14(a) and 14(b), we plot the effective domain growth exponent n as a function of temperature for the square lattice with $Q=6$ and 36, respectively. While the effective growth exponent is zero at $T=0$ on the square lattice for $Q \geq 3$, with increasing temperature, n approaches the growth exponent found for the identical Q on the triangular lattice. The transition to the lattice-independent exponent occurs at a lower normalized temperature (T/T_c) for $Q=6$ than for $Q=36$ since T_c decreases with increasing Q and the thermal fluctuations are T_c independent. These results suggest the presence of universal or lattice-independent kinetics at temperatures below T_c.

As was discussed above, the slowing down of the kinetics by domain pinning is due to the removal of kinks or

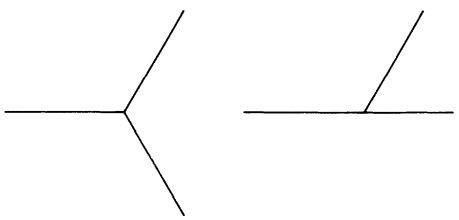

FIG. 10. Two possible vertex configurations on a triangular lattice. Only the first configuration is stable.

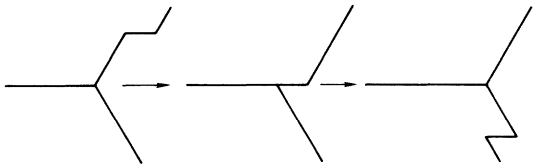

FIG. 11. Schematic illustration of a vertex-kink reaction on the triangular lattice. A kink traveling down one of the boundaries is transmitted through, rather than being absorbed by, the vertex.

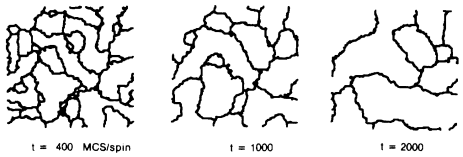

FIG. 13. Spin configurations for the $Q=4$ Potts model on a square lattice that was quenched from $T \gg T_c$ to $T=0.6T_c$. These configurations more closely resemble the configurations of the triangular lattice Potts models (Figs. 2 and 12) than the low-temperature square lattice Potts models (Fig. 7).

curvature by certain types of vertices. With increasing temperature the kink absorption at the vertices is compensated by the thermal generation of kinks due to the roughening of the domain walls by thermal fluctuations. As a result of the roughening, the difference in kink density between boundaries on square and triangular lattices is reduced with increasing temperature. Pinning by vertices is less effective for low-Q values than for large-Q values, since for small Q, growth by coalescence may also be important. Therefore, the transition from logarithmic growth to power-law growth should occur at a characteristic temperature that decreases with decreasing Q. Comparisons of these temperatures for $Q=6$ and 36 (Fig. 14) show that this is indeed the case.

C. Discussion

While the kink-absorbing properties of the square lattice can be overcome by the thermal generation of kinks, the square lattice can be unpinned in a completely different manner. By generalizing the Potts Hamiltonian [Eq. (1)] to include second-nearest-neighbor interactions of strength equal to that for the first-nearest-neighbor interactions we were able to unpin the square lattice. Even though kinks are still absorbed by vertices, the generation of certain types of kinks at the vertices is a $\Delta E=0$ process. Since in this case the vertices act as kink sources, in a manner analogous to the spontaneous kink generation along the boundaries at elevated temperatures, we should expect that the kinetics of this model should be identical to those of the square lattice Potts model with first-nearest-neighbor interactions in the high-temperature limit. $T=0$ simulations on the square lattice with this modified Hamiltonian show the same kinetic exponent as was observed on the triangular lattice (first-nearest-neighbor interactions) at $T=0$ and the high-temperature limit of the first-nearest-neighbor square lattice. This result further indicates the presence of lattice-independent kinetics, provided that local pinning can be circumvented.

The higher-order topological connectedness that exists in high-Q systems introduces kinetic effects that are not possible in simpler, $Q<d+1$, systems. In the simpler or Ising-type systems, barring coalescence, the motion of one boundary is unaffected by the motion of any other boundary. In such a case the dynamics of a boundary is governed by its own curvature. On the other hand, for higher Q, the domains are coupled through the vertices. For example, the shrinking of one domain might rotate a vertex. Such a rotation will change the curvature on all three boundaries that meet at that vertex. Similarly, a kink propagating down one boundary to a vertex can rotate the vertex (see Fig. 15), instead of being translated through the vertex onto a second boundary. The partial vertex rotation shown in Fig. 15(b), can be completed by

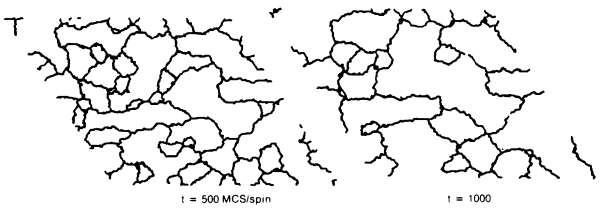

FIG. 12. Spin configurations for the $Q=4$ Potts model on a triangular lattice that was quenched from $T \gg T_c$ to $T=0.6T_c$.

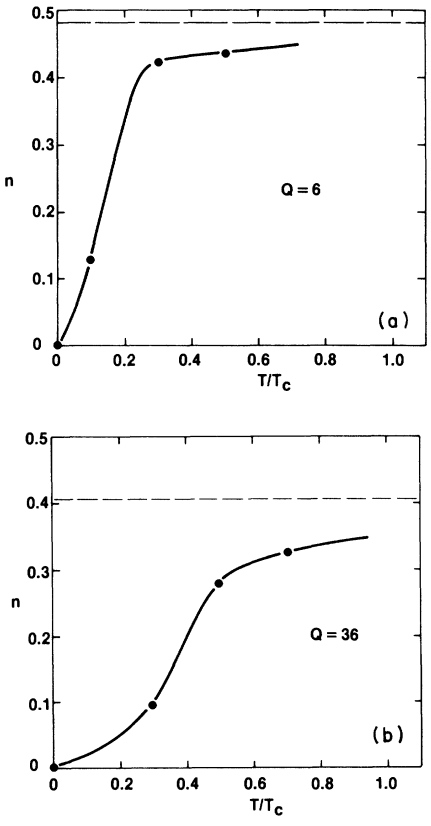

FIG. 14. Temperature dependence of the effective domain growth exponent n on the square lattice Potts model for $Q=6$ (a) and for $Q=36$ (b).

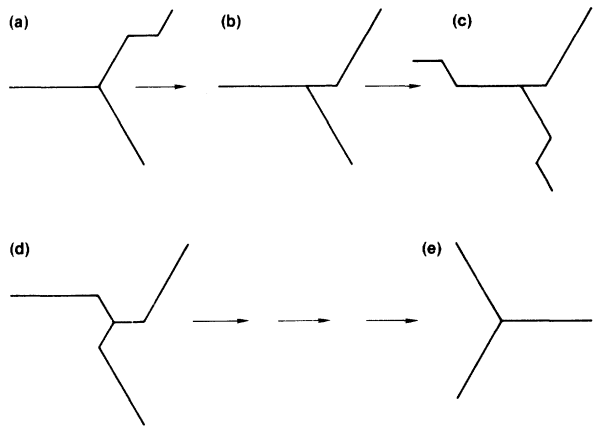

FIG. 15. Schematic illustration of a vertex rotation by a kink absorption mechanism. A kink moving down one of the boundaries (a), stops at the vertex (b). In order to restore the 120° boundary condition, the vertex can absorb one kink from each of the other two boundaries (c), thereby completing the vertex rotation (d). If additional kinks of proper orientation arrive at the rotated vertex, the boundaries can be straightened (e).

the absorption of one additional kink from each of the other two boundaries meeting at that vertex [Figs. 15(c)–15(d)]. The arrival of additional kinks are capable of rotating the entire three-domain structure [Fig. 15(e)]; however, this is unlikely for the quench case since each domain is connected to other vertices as well. While kink annihilation at vertices control the kinetics of domain growth on the square lattice at $T=0$ (Fig. 8), at higher temperatures, where the kink annihilation properties of the vertices are less important, vertex rotation through kink absorption will become an important process [see Fig. 9(b)] just as it is on the triangular lattice at all temperatures. Therefore, since curvature or, equivalently, kinks are removed from the system by vertex rotations, the advent of such rotations should slow the kinetics of domain growth. Furthermore, since domains are connected at the vertices, it is possible to redistribute curvature from one domain to another via rotations. The kinetics of such rotations-redistributions may differ from that of pure curvature-driven growth, thereby modifying the domain growth exponent for the large, multidomain aggregate. It may be concluded, therefore, that the decrease in the domain growth exponent with increasing Q, the differences between the square and the triangular lattices at $T=0$, as well as their equivalence at elevated temperatures are all explainable in terms of interactions that occur at the domain vertices. While the kinetics of the $Q=2$ (Ising) model is describable purely in terms of curvature, the presence of vertices ($Q \geq d+1$) introduces nonlocal curvature effects. Such effects should become increasingly important as the relative density of vertices increases. This relative density is given by the number of vertices per unit length of boundary or, provided that the domains grow in a time invariant manner (see below) this is given in time invariant form by the ratio of the perimeter to the domain radius R since the mean number of vertices per domain is 6 for $d=2$. This is considered in more detail in Sec. IV, where the domain topology is considered explicitly.

Experience with previous domain growth theories[19] and Ising models[5,6] suggests that the exponent n is identical in two and three dimensions. While the verification of this conjecture is currently being pursued, comparison with existing data in the high-Q or grain growth limit ($Q=\infty$) can be made. Such comparisons, however, are difficult since values of the domain growth exponent n vary over a wide range (0–0.5). Additional complications arise because many authors have analyzed their data by plotting the left-hand side of Eq. (10) against t, for particular values of m, so as to facilitate comparison with theories that predict a growth exponent n of $\frac{1}{2}$ or $\frac{1}{3}$. Furthermore, experimental studies of grain growth in metals often show grain growth exponents that are temperature dependent; however, this has usually been attributed to the presence of impurities. Therefore, limiting ourselves to zone-refined metals which show temperature-independent growth exponents over the temperature range of the experiments, we find two studies on lead[26,27] which yield exponents of 0.40 and 0.41, one study on tin[27] with an exponent of 0.432 and one on aluminum[28] giving 0.25. While admittedly this sampling is limited and the variation of exponents quoted is wide, we find that the average of these exponents, 0.37 ± 0.07, is in reasonable agreement with that found for the Potts model in the high-Q limit. A sampling of the ceramic grain growth data shows that for ZnO,[29] it is $\frac{1}{3}$; for MgO,[30,31] $\frac{1}{2}$ and $\frac{1}{3}$; for CdO,[32] $\frac{1}{3}$; for $Ca_{0.16}Zr_{0.84}O_{1.84}$,[33] 0.4; and for UO_2,[34] $\frac{1}{3}$. Unfortunately, in the cases where the exponents are indicated as fractions, the exponents were obtained using Eq. (10), where usually only one or two integer m values were checked. However, the average of these exponents is 0.37 ± 0.06, again, in reasonable agreement with our results on the high-Q Potts model. These results contrast with the predictions of most grain growth theories,[19,35] which invariably predict exponents of $\frac{1}{2}$, presumably due to neglect of vertex effects.

IV. SIZE DISTRIBUTION AND TOPOLOGY OF GRAINS

In this section we report the results of a detailed cluster analysis for $Q=3$, 6, 12, 36, and 64 on a triangular lattice at $T=0$, and $Q=36$ on a square lattice at $T=0.6T_c$. We have evaluated two distinct types of parameters associated with each domain: (i) the extensive parameters such as area A, perimeter S, and effective radius R, and (ii) the topological parameter N_e, number of domain edges. The parameters are determined from the simulation data employing a computer code in which (i) the domain area is measured by counting the number of sites which have at least one nearest neighbor of the same orientation, (ii) the perimeter is measured by adding the number of sites which have at least one nearest neighbor with a different orientation, and (iii) the number of domain edges is measured by counting the various neighboring domains which share boundaries with the domain under consideration. The effective radius is calculated from the domain area using $R=\sqrt{A/\pi}$.

The cluster analysis was carried out for each Q as a function of time. The domain area distribution was then

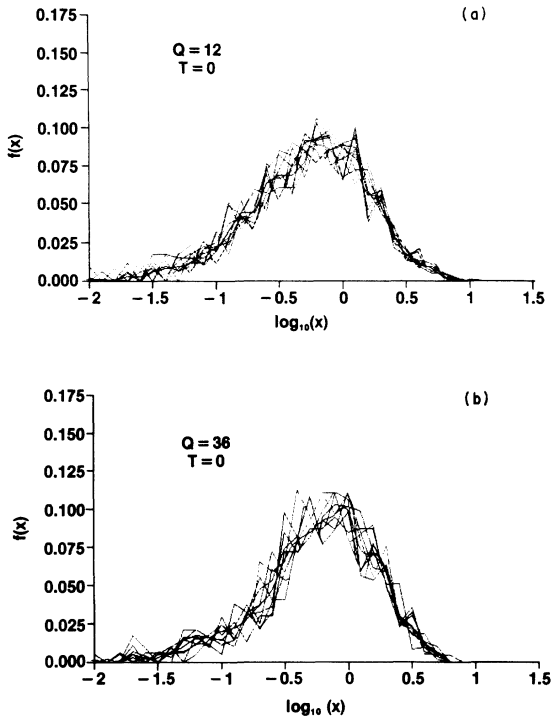

FIG. 16. Size distribution function $f_Q(\log_{10}x)$ for different times for (a) $Q=12$ and (b) $Q=36$ on triangular lattice at $T=0$.

examined by plotting the frequency of occurrence f versus the logarithm of the normalized area $x=A(t)/\bar{A}(t)$ where $\bar{A}(t)$ is the mean domain area at time t. In Figs. 16(a) and 16(b) we plot the area distributions at fifteen different times for $Q=12$ and 36, respectively. We observe that for all $Q\geq 3$ the scaled curves are time invariant within the statistical error of our simulations. The time-averaged domain area distributions for $Q=3$, 6, 12, 36, and 64 are presented in Figs. 17(a)–17(e). To observe time invariance for $Q=2$, one requires lattice sizes much larger than our present storage capacity allows.

The mean μ and standard deviation σ of $f_Q(\log_{10}x)$ and the standard deviation of $f_Q(x)$, σ_x, for different Q are listed in Table I. The distribution $f_Q(x)$ is characterized by a mean of one, independent of Q (this is due to the definition of x). The standard deviation of $f_Q(x)$ on the triangular lattice decreases from $\sigma_x\cong 2$ for Q small to the limiting value $\sigma_x\cong 1$ as Q becomes large. We also note that $f_Q(x)$ for $Q=36$ is congruent (within statistical error) with $f_Q(x)$ for $Q=64$. This is consistent with the behavior of the growth exponent n on the triangular lattice, which has the limiting value $n\cong 0.41$ for $Q>30$. Moreover, we find that $f_Q(x)$ for $Q=36$ on the triangular lattice is also congruent (within statistical error) with $f_Q(x)$ for $Q=36$ on the square lattice, in the high-temperature limit where the growth exponent for the square lattice also approaches $n\cong 0.41$ [Fig. 18]. We conclude from these results that the domain area distribution $f_Q(x)$ has the limiting form $F(x)$ as Q becomes sufficiently large. $F(x)$ is independent of the lattice in the temperature regime where the growth exponent is independent of lattice ($n\cong 0.41$), and is characterized in part by

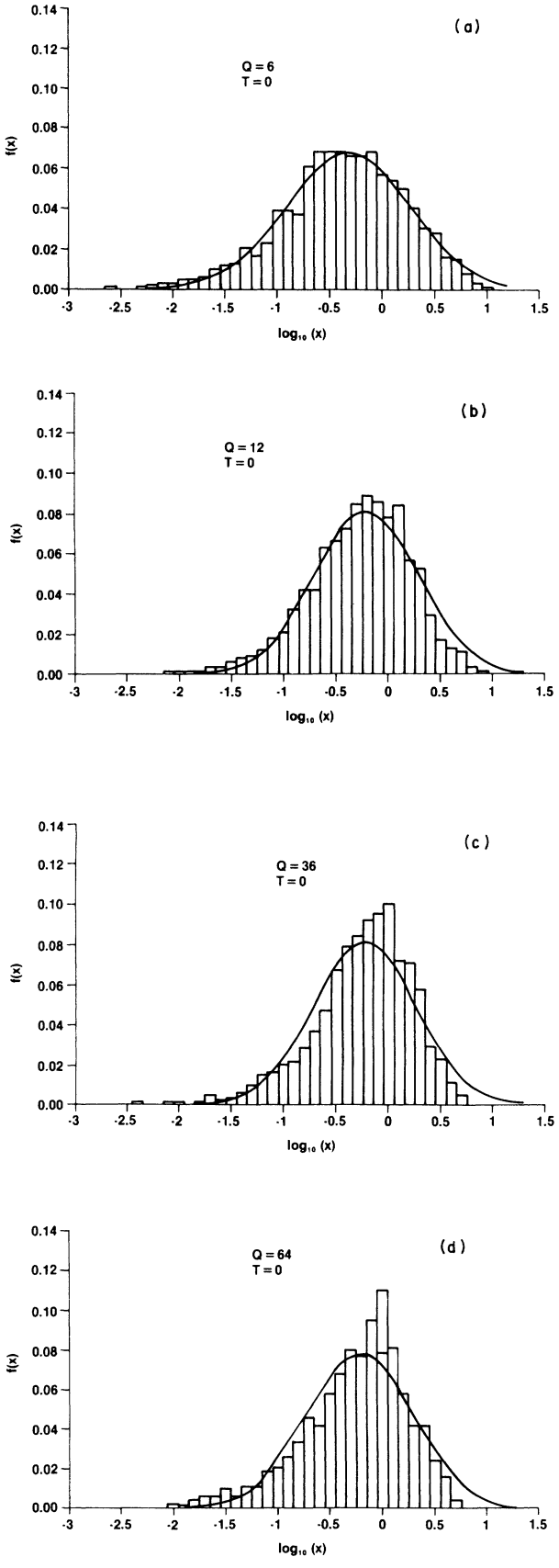

FIG. 17. Averaged size distribution function $f_Q(\log_{10}x)$ for (a) $Q=6$, (b) $Q=12$, (c) $Q=36$, and (d) $Q=64$. The solid line corresponds to log-normal function with the appropriate values of σ and μ taken from Table I for different Q's.

TABLE I. The mean μ and standard deviation σ of $f_Q(\log_{10}x)$ and the standard deviation σ_x of $f_Q(x)$ are tabulated for systems quenched from $T \gg T_c$ to $T=0$ on the triangular lattice.

Q	μ	σ	σ_x
3	−0.48	0.70	1.72
6	−0.33	0.58	1.34
12	−0.23	0.49	1.09
36	−0.21	0.49	0.95
64	−0.22	0.50	0.96

$\mu_x=\sigma_x=1$. The existence of a limiting distribution supports the assumption that large-Q Potts models can be used to describe the $Q=\infty$ Potts model. Furthermore, the observation of the lattice independence of n and $F(x)$ under appropriate conditions ($Q>30$ and $T>0.6T_c$ in this study) suggests that growth characteristics of the large-Q Potts model are universal (at sufficiently high temperature). This provides the motivation for modeling domain growth in polycrystalline metals and ceramics by identifying Q with the grain orientation.

Comparison of $F(\log_{10}x)$ with domain area data taken from the literature is given in Fig. 19. The experimental data consist of the domain diameter distribution measured for two-dimensional cross sections of three-dimensional specimens of high-purity Al (Ref. 35) and the ceramic MgO.[36] For these materials it is observed that (i) the diameter distribution is time invariant when plotted as a function of $D/\bar{D}$ ($D=2\sqrt{A/\pi}$), and (ii) the form of the distribution (over the range of sizes in which the data could be collected) is nearly log normal. The log-normal fit to the actual data is plotted. We note that good agreement is obtained between the simulation distribution and the experimental data. In particular, the maximum domain size found in the simulation ($D/\bar{D}\cong 2.8$) agrees with these data and general observations in metals[35] and ceramics.[36]

Our understanding of the correspondence between the simulation results and the two-dimensional measurements of three-dimensional domain distributions is not complete. However, the above results are consistent with theory and observation of grain growth in polycrystalline materials. First, the mean-field treatment of grain growth[19] predicts nearly identical size distributions for two- and three-dimensional growth (although the shape and exponent of the mean-field distributions disagree with experiment, e.g., Fig. 19). Second, Feltham[35] has shown that for the log-normal function the planar distribution of diameters measured from two-dimensional cross sections closely represents the spatial distribution of grain diameters.

While $F(\log_{10}x)$ is in fair correspondence with the log-normal shape, there are two important differences. First, the log-normal function is symmetric with tails extending to $\pm\infty$. However, $F(\log_{10}x)$ is skewed, and has an upper cutoff at $x\cong 2.8$. Second, $F(\log_{10}x)$ peaks more sharply than does the log-normal distribution. We find that the log-normal form is a better representation of the simulation distribution for small Q. A comparison of $F_Q(\log_{10}x)$ and the log-normal function computed using the parameters of Table I for each Q are plotted as continuous curves in Figs. 17(a)—17(d). The development of the log-normal distribution in domain growth has been rationalized in terms of a probabilistic mechanism in which individual domains are assumed to change area (or volume) in a random and uncorrelated fashion.[37] This argument is not appropriate in the high-Q limit, where the density of vertices is high. The presence of vertices couples each domain to its neighbors, so that changes in area (or volume) are correlated. Deviations from the log-normal distribution are therefore to be expected. However, in the low-Q limit, the density of vertices decreases and the correlation between domains becomes smaller. In this case the assumptions of the argument are better satisfied, and the log-normal distribution should be a better fit. This is in fact what we observe [Figs. 17(a)—17(d)]. Moreover, the lack of vertices in the Ising case ($Q<d+1$) implies completely uncorrelated growth (except for area conservation requirements) and would also be expected to show a log-normal domain size distribution.

We have analyzed the topology by monitoring the num-

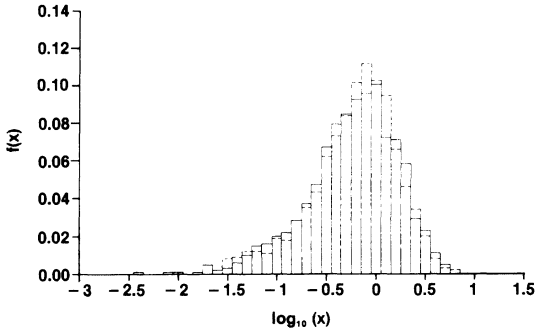

FIG. 18. Same as in Fig. 17 for $Q=36$ on triangular lattice (solid line) at $T=0$ and on square lattice (dotted line) at $T=0.6T_c$.

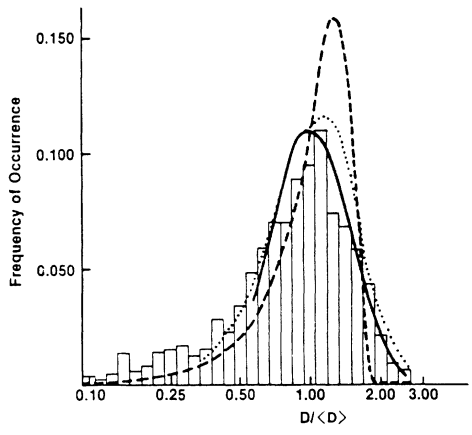

FIG. 19. Comparison of grain size distribution from the present simulations (histogram) with the experimental data for high-purity Al (solid line) and MgO (dotted line). The dashed line is predicted by Hillert (Ref. 19).

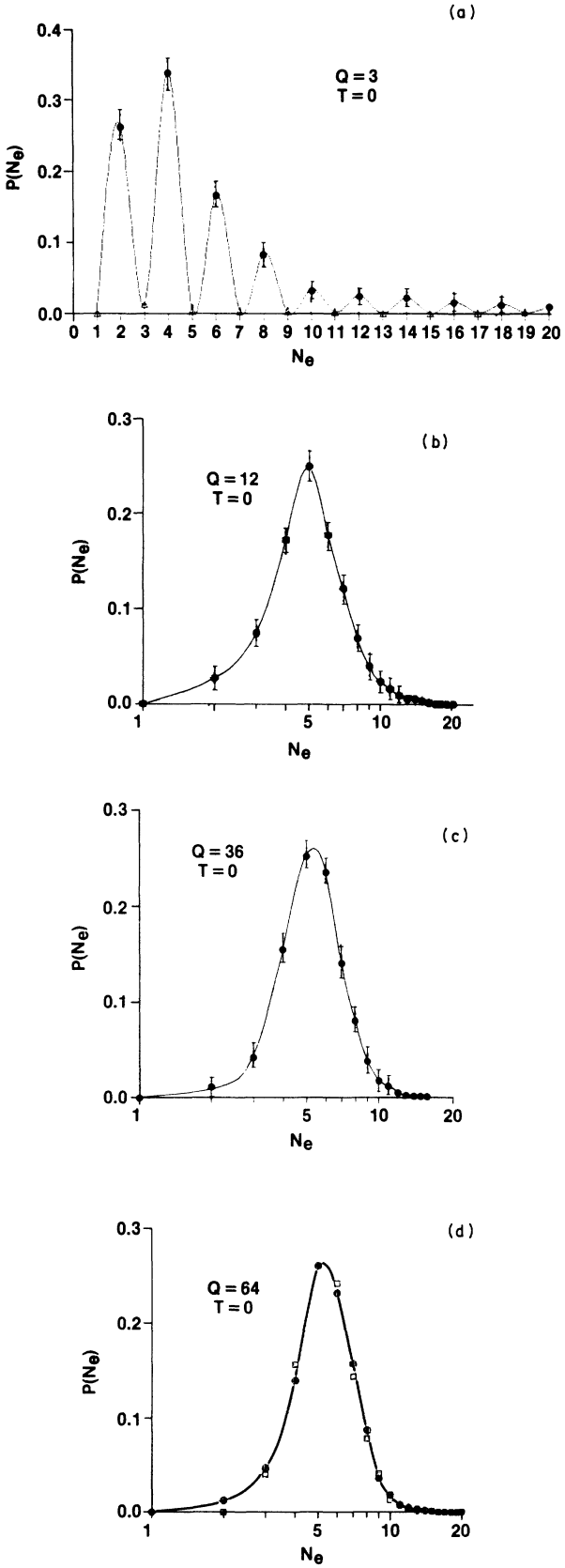

FIG. 20. Distribution function for the number of edges per grain plotted on a semilog scale for $Q=3$, 12, 36, and 64. The bars correspond to the maximum deviation observed for different times from the averaged curve. For $Q=64$, the data for pure Al (squares) is compared with present simulations.

ber of edges per grain N_e. We plot the frequency distribution $P(\log_{10}N_e)$ for $Q=3$, 6, 12, 36, and 64 [Figs. 20(a)–20(d)]. We find that $P(\log_{10}N_e)$ is time invariant, as was observed for the area distribution. For $Q>3$, $P(\log_{10}N_e)$ is approximately log normal. Further, we observe that $P(\log_{10}N_e)$ for $Q=36$ is congruent with $P(\log_{10}N_e)$ for $Q=64$. This implies that $P(\log_{10}N_e)$ approaches a limiting form with increasing Q, in agreement with the behavior of $f_Q(\log_{10}x)$ and the growth exponent n. However, for $Q=3$, we obtain an interesting multipeaked distribution function with peaks located at even N_e values. This is a consequence of the fact that a domain of a given orientation can only be surrounded by domains of the other two orientations in alternating order. Such a multipeaked distribution function will always be observed for $Q=d+1$.

We have divided $F(\log_{10}x)$ into the contributions from the separate topological classes (Fig. 21). We note that the peak of $F(\log_{10}x)$ is dominated by 5-, 6-, and 7-sided domains. This is not surprising since the most probable domain morphology has five sides [Fig. 20(d)], while the mean number of sides must be six (from space-filling constraints). The mean radius for each topological class versus the class number N_e is plotted in Fig. 22. We observe that a linear relationship exists between domain radius and the number of sides per domain, as suggested by the similarity of the domain edge distribution and the domain area distribution. The forms of the domain edge distribution and the topologically divided domain size distribution, and the linear relationship between domain radius and number of edges, are all in good agreement with observations on the grain structure of polycrystalline metals.[38]

As discussed in Sec. III on kinetics, the degree of domain asymmetry is large at low Q, with domains becoming more equiaxed and compact as Q is increased. A convenient measure of the domain irregularity (and boundary unevenness) is the ratio K of the mean domain perimeter S divided by the mean domain radius R. The quantity K is large for irregular or ramified domains, and approaches 2π as the domain morphology becomes more circular. We note that the time invariance demonstrated by the domain area distribution for $Q\geq 3$, coupled with

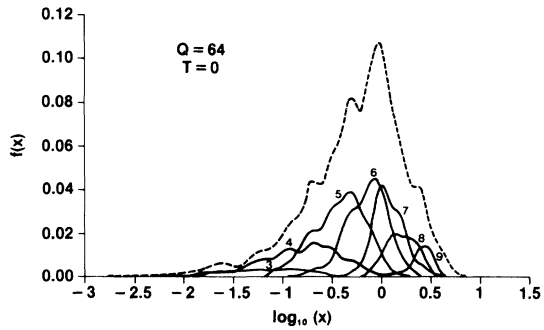

FIG. 21. Size distribution function $f_Q(x)$ plotted for $Q=64$ on triangular lattice at $T=0$ for different topological classes.

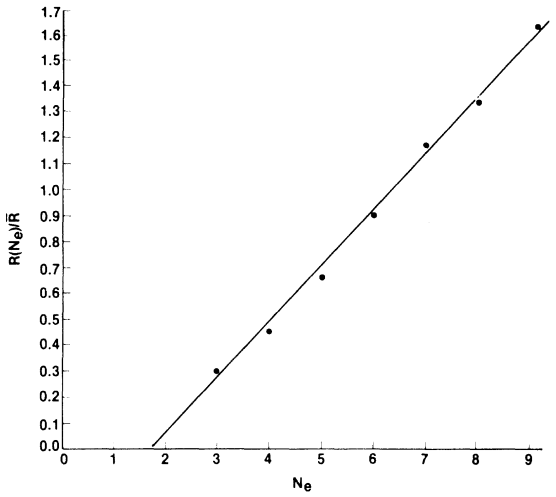

FIG. 22. Mean radius for each topological class vs N_e.

the compact domain shape caused by a high vertex density, suggests that for high Q, K is a constant of growth. Moreover, by substituting $\bar{A}=A_T/N$ where A_T is the total area and N is the total number of domains, we find that the total boundary length S is related to N by $S\cong K\sqrt{A_T/4\pi N}$. This implies that the total number of domains (or mean area) can be followed by measuring the total boundary length alone (provided sufficient time passes for the steady-state area distribution to be established). Since the total energy is approximately proportional to the total boundary length, the number of domains (or mean area) can also be monitored via the total energy. The exponent n obtained by monitoring energy agrees well with that obtained via monitoring vertices.

V. CONCLUSIONS

In summary, a detailed Monte Carlo study has been presented for the kinetics of domain growth in two-dimensional systems for both small ($Q=3,4,6$) and large ($Q=12-64$) degeneracies. The average linear domain size R is shown to grow as $R\sim t^n$ where $n=0.5$ for $Q=2$ and $n=0.41$ for large Q. On the square lattice, with short-ranged interactions, the growth exponent is zero at low temperatures, but approaches the apparently universal value of 0.41 at high temperatures. An analysis of the distribution of domain sizes and shapes demonstrates the time invariance of these distributions for high Q. The distributions obtained from the simulations are in good agreement with the experimental results for domain growth in polycrystalline materials.

[1]P. S. Sahni and J. D. Gunton, Phys. Rev. Lett. 47, 1754 (1981).
[2]M. G. Lagally, G. C. Wong, and T. M. Lu, CRC Crit. Rev. Solid State Mat. Sci. 7, 233 (1978).
[3]J. E. Burke and D. Turnbull, Prog. Metal Phys. 3, 220 (1952).
[4]S. M. Allen and J. W. Cahn, Acta Metall. 27, 1085 (1979).
[5]M. K. Phani, J. L. Lebowitz, K. H. Kalos, and O. Penrose, Phys. Rev. Lett. 45, 366 (1980).
[6]P. S. Sahni, G. Dee, J. Gunton, M. Phani, J. L. Lebowitz, and M. Kalos, Phys. Rev. B 24, 910 (1981).
[7]S. A. Safran, P. S. Sahni, and G. S. Grest, preceding paper, Phys. Rev. B 28, 2693 (1983).
[8]P. S. Sahni, G. S. Grest, and S. A. Safran, Phys. Rev. Lett. 50, 60 (1983).
[9]The Potts model is expected to be most applicable to polycrystals with high angle grain boundaries.
[10]I. M. Lifshitz, Zh. Eksp. Teor. Fiz. 42, 1354 (1962) [Sov. Phys.—JETP 15, 939 (1962)].
[11]J. W. Sacco and J. Chalupa, Solid State Commun. 39, 75 (1981).
[12]J. R. Banavar, G. S. Grest, and D. Jasnow, Phys. Rev. Lett. 45, 1424 (1980).
[13]O. G. Mouristen and A. J. Berlinsky, Phys. Rev. Lett. 48, 181 (1982).
[14]A. N. Berker, S. Ostlund, and F. A. Putnam, Phys. Rev. B 17, 3650 (1978).
[15]G. S. Grest, S. A. Safran, and P. S. Sahni, J. Magn. Magn. Mater. 31-34, 1011 (1983).
[16]P. S. Sahni, G. S. Grest, M. P. Anderson, and D. J. Srolovitz, Phys. Rev. Lett. 50, 263 (1983). In this paper we reported a slightly lower value of the exponent n. The difference is due to a slight programming error which has since been corrected.
[17]The correspondence between the Potts model and the surface ordering problem was discussed in the preceding paper.
[18]F. Haessner and S. Hofman, in *Recrystallization of Metallic Materials*, edited by F. Haessner (Riederer, Stuttgart, 1978), p. 63.
[19]M. Hillert, Acta Metall. 22, 721 (1974).
[20]*Monte Carlo Methods in Statistical Physics*, edited by K. Binder (Springer, Berlin, 1979).
[21]A. B. Bortz, M. H. Kalos, and J. L. Lebowitz, J. Comput. Phys. 17, 10 (1975).
[22]T. Graim and D. P. Landau, Phys. Rev. B 24, 5156 (1981).
[23]D. J. Srolovitz, M. P. Anderson, G. S. Grest, and P. S. Sahni, Scripta Metall. 17, 241 (1983).
[24]S. A. Safran, Phys. Rev. Lett. 46, 1581 (1981).
[25]D. Harker and E. A. Parker, Trans. Am. Soc. Met. 34, 156 (1945).
[26]G. F. Bolling and W. C. Winegard, Acta Metall. 6, 283 (1958).
[27]J. P. Drolet and A. Galibois, Acta Metall. 16, 1387 (1968).
[28]P. Gordon and T. A. El-Bassyouni, Trans. AIME 233, 391 (1965).
[29]S. K. Dutta and R. M. Spriggs, J. Am. Ceram. Soc. 53, 61 (1970).
[30]C. M. Kapadia and M. H. Leipold, J. Am. Ceram. Soc. 57, 41 (1974).
[31]R. S. Gordon, D. D. Marchant, and G. W. Hollenberg, J. Am. Ceram. Soc. 53, 399 (1970).
[32]V. Petrovic and M. M. Ristic, Metallography 13, 219 (1980).
[33]T. Y. Tien and E. C. Subbarao, J. Am. Ceram. Soc. 46, 489 (1963).
[34]W. D. Kingery and B. Francois, J. Am. Ceram. Soc. 48, 546 (1965).
[35]P. Feltham, Acta Metall. 5, 97 (1957).
[36]D. A. Aboav and T. G. Langdon, Metallography 1, 335 (1969).
[37]S. K. Kurtz and F. M. A. Carpay, J. Appl. Phys. 51, 5725 (1980).
[38]F. N. Rhines and K. R. Craig, Met. Trans. 5, 413 (1974).

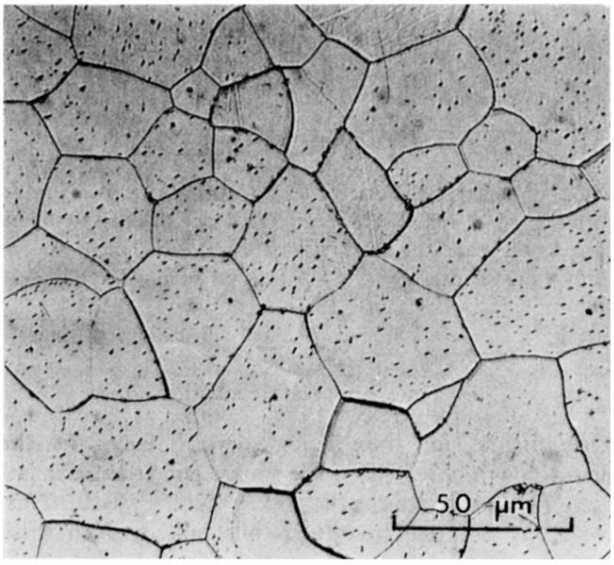

FIG. 4. Cross section of a high-purity polycrystalline iron sample which was etched to highlight the grain boundaries.